Inorganic Chemistry

ARTICLE

pubs.acs.org/IC

Structural Study of a Series of Layered Rare-Earth Hydroxide Sulfates

Fengxia Geng,[†] Renzhi Ma,[†] Yoshitaka Matsushita,[§] Jianbo Liang,[†] Yuichi Michiue,[‡] and Takayoshi Sasaki*[,†]

[†]International Center for Materials Nanoarchitectonics and [‡]Quantum Beam Center, National Institute for Materials Science, 1-1 Namiki, Tsukuba, Ibaraki 305-0044, Japan

[§]Beamline Station, National Institute for Materials Science, 1-1-1 Kouto, Sayo-cho, Sayo-gun, Hyogo 679-5148, Japan

Supporting Information

ABSTRACT: We report structure analysis of a new family of rare-earth hydroxides $Ln_2(OH)_4SO_4\cdot 2H_2O$ (Ln = Pr, Nd, Sm, Eu, Gd, Tb) from synchrotron X-ray and electron diffraction data. Rietveld profile analysis revealed that all members were isostructural and crystallized in a face-centered monoclinic system $A2/m$ (No. 12), in which the monoclinic angles were approximately equal to the right angle, varying from 90.387(1)° for Pr sample to 90.0718(3)° for Tb sample. The structure consisted of LnO_9 polyhedra connected by μ_3-hydroxyl groups and μ_2-water molecules, forming a corrugated two-dimensional layer, which was pillared by bidentated sulfate ions. This series of compounds had a supercell $a' = 2a$, $b' = 2b$ because of the local orientation ordering of SO_4^{2-}. Structural features along the series, such as unit-cell parameters and average Ln−O distances, represented a progressive contraction associated with the shrinking radius of the lanthanide cations from Pr to Tb.

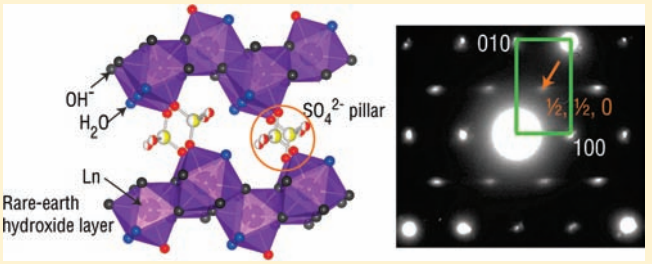

INTRODUCTION

Layered rare-earth hydroxides have been of great interest because of the unique combination of advantages of lanthanide (Ln) cations in the host and exchangeable anions and the existence of a plethora of possible structure types.[1−3] Recently, considerable attention was given to $Ln_2(OH)_5X\cdot mH_2O$ (X = Cl^-, Br^-, NO_3^-, etc., m = 0−2) because of their structure similarity to a well-known anion-exchangeable material, layered double hydroxides (LDH), and the corresponding facile anion exchangeability.[4−10] They have found applications in numerous fields ranging from optical devices,[11,12] catalyst,[13] to medical uses.[14,15] High-crystalline powder materials or single crystals, in some instances, were obtained with incorporated anions such as Cl^-, NO_3^-, Br^-, and organic anions like cyclic disulfonate. Their structures can be generally described as alternate packing of positively charged layers of lanthanide polyhedra with 8 or 9 coordinations and exchangeable anions in the gallery. However, depending on the identity of incorporated anion, the crystallized symmetry varies from monoclinic to orthorhombic, and packing of both one- and two-layer repetition is present.

The structural variations motivated us to revisit hydroxides with a different composition $Ln(OH)_2X\cdot nH_2O$ (X = Cl^- or NO_3^-; n = 0 or 1) to understand the relationship between the composition and the structure of these materials and the interactions between layered host and guest anions. Structural study of this class of materials was extensively performed in the 1970s. $Ln(OH)_2Cl$ was reported to consist of stacking of neutral slabs composed of $Ln(OH)_6Cl_2$ polyhedra in monoclinic or orthorhombic symmetry.[16,17] $Ln(OH)_2NO_3\cdot nH_2O$ exhibits layers formed by polyhedra of 9-coordinated metal centers, with the nitrate group acting as a monodentate ligand in $Ln(OH)_2NO_3\cdot H_2O$ or a bidentate ligand in $Ln(OH)_2NO_3$.[18,19] Recently, the structure evolution of $Ln(OH)_2Cl$ was examined across the lanthanide series from Nd to Lu.[20] Different from monovalent anion, spherical Cl^- or planar NO_3^-, SO_4^{2-} is divalent and has a tetrahedral geometry, which makes it possible to produce a different structure. However, the synthesis of sulfate members of high crystallinity for structural analysis was not successful until recently.[21] In our laboratory, layered rare-earth hydroxide sulfates, $Ln_2(OH)_4SO_4\cdot 2H_2O$ (Ln = Pr, Nd, Sm, Eu, Gd, and Tb), grown as elongated platelets with edge lengths of up to several micrometers, were obtained using a homogeneous precipitation method.[22] In this paper, we report the structure determination and analysis of $Ln_2(OH)_4SO_4\cdot 2H_2O$ for this series, which reveals an interesting stacking of lanthanide layers pillared by bidentated sulfate ions. In addition, the structural trends across the series, including unit-cell dimensions, bond distances, and sulfate distortions, are also fully addressed.

EXPERIMENTAL SECTION

Materials Preparation. The synthesis of $Ln_2(OH)_4SO_4\cdot 2H_2O$ (Ln = Pr, Nd, Sm, Eu, Gd, Tb) was performed according to our previously reported procedures.[22] A mixture of 5 mmol of the corresponding rare-earth sulfate salt $Ln_2(SO_4)_3\cdot 8H_2O$ (Aldrich, 99.99%), 25 mmol of Na_2SO_4 (Wako, >99.5%), and 1.8 mmol of HMT (Wako, >99.5%) in 1000 cm^3 of Milli-Q filtered water was loaded into a two-neck flask and then connected to a reflux condenser. The solution was

Received: March 22, 2011
Published: June 10, 2011

subsequently heated at a refluxing temperature under nitrogen flow for 6 h. The as-precipitated powder was separated by filtration, washed with distilled water to remove any possible ionic remnants, and then dried in a box with relative humidity set at 75%.

Electron Diffraction. The selected-area electron diffraction (SAED) pattern was taken on a JEOL JEM-1010 transmission electron microscope working at 100 kV. The sample was prepared by dispersing a small amount of powder in ethanol using sonication. A few drops of the resulting suspension were deposited onto a carbon-coated grid and dried for observation.

Structure Determination. The synchrotron powder diffraction data were collected by a high-resolution diffractometer on BL15, Spring-8 Synchrotron radiation facility, Japan. The samples were packed into 0.2 mmϕ Lindenmann tube capillaries, and data collection was performed with a monochromatic wavelength of $\lambda = 0.65297$ Å at ambient conditions. Unit-cell parameter determination was carried out with various programs: ITO,[23] DICVOL,[24] and TREOR[25] methods and refined with APPLEMAN.[26] The structure was solved by direct methods with EXPO2004[27] and refined by the full-profile Rietveld fitting program RIETAN-2000.[28] The structure model was modified and completed referring to the electron density distribution that was determined by the maximum-entropy method (MEM) embedded in RIETAN-2000.[29] Isotropic temperature factors were added for refinement when reliability indices no longer decreased appreciably and the structure model agreed well with electron density maps. The ultimate refined fractional atomic coordinates along with site occupancy and refinement statistics for the various $Ln_2(OH)_4SO_4 \cdot 2H_2O$ phases are listed in the Supporting Information.

RESULTS AND DISCUSSION

Unit-Cell Determination. Synchrotron X-ray diffraction patterns recorded at room temperature gave sharp lines, suggesting their highly crystalline nature. Tb sample gave significantly higher quality powder diffraction pattern, and thus, it was chosen for initial structural investigation. ITO,[23] DICVOL,[24] and TREOR[25] methods were used to find a preliminary cell. The cell with the highest symmetry was orthorhombic with approximate dimensions $a = 6.232$ Å, $b = 3.706$ Å, and $c = 16.620$ Å. Two strong peaks in the low-angle area can be indexed as *002* and *004* reflections, suggesting that one unit cell contains two layers with a separation distance of 8.3 Å. The cell was used to index the diffraction pattern, and it was found that almost all the peaks could be incorporated (Figure 1a). The cell is close to the one proposed in our previous report[22] except for a difference in axis notation. However, close scrutiny of the diffraction profile revealed a splitting for some peaks in the higher angular region, for example, *317* reflection near $2\theta \approx 26.20°$ and *319* reflection near $2\theta \approx 29.25°$, as illustrated in Figure 1b, which indicates a lower symmetry, e.g., monoclinic. In practice, cell parameters refinement using structure-free full-profile fitting in RIETAN gave rise to an extremely subtle monoclinic distortion, characterized by a β angle of 90.072°. All peaks were then satisfactorily incorporated, and the above-mentioned two components of the split peaks at ~26.20° and 29.25° can be indexed as *317*/$\bar{3}$*17*, and *319*/$\bar{3}$*19*, respectively. The indexing revealed the extinction condition as $k + l = 2n + 1$ for general *hkl* reflections, which was assigned to an *A*-centered lattice, leading to the following space groups: *A*2 (No. 5), *Am* (No. 8), and *A*2/*m* (No. 12). The fact that *a* is close to $\sqrt{3}$b recalls the structure of $Tb_2(OH)_5Cl \cdot 2H_2O$, in which some displacement of Tb atoms from hexagonal arrangement results in a larger cell. The Tb···Tb distance is ~3.65 Å. Supposing that Tb has a similar quasi-hexagonal arrangement, each unit layer contains 2 Tb atoms,

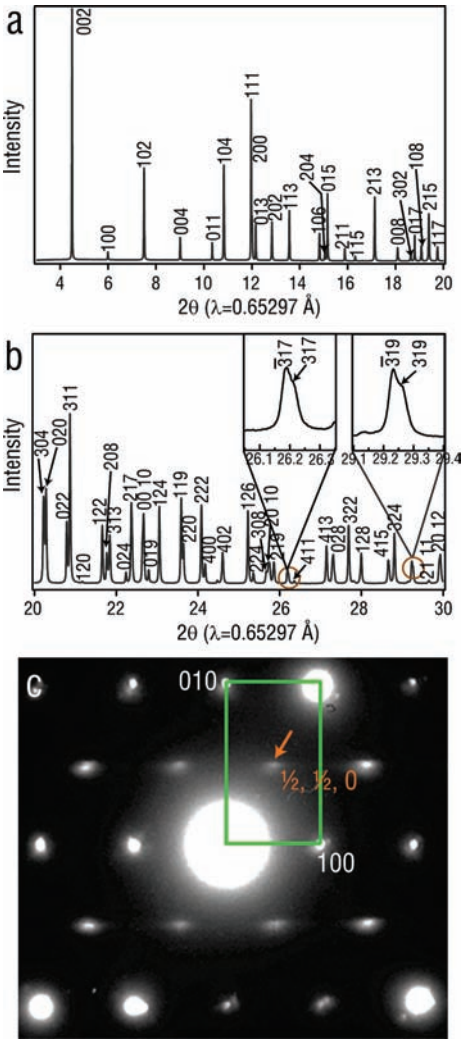

Figure 1. Indexing of the synchrotron diffraction pattern of $Tb_2(OH)_4SO_4 \cdot 2H_2O$ (a) from 3° to 20° and (b) from 20° to 30°. Insets in b show examples of splitting peaks that cannot be fully indexed with an orthorhombic cell and their indices in the monoclinic cell. (c) SAED pattern taken along the [001] zone axis. The orange arrow indicates the superspot.

i.e., the number of formula units of $Tb(OH)_2(SO_4)_{0.5} \cdot H_2O$ in the unit cell is 4.

SAED characterization (Figure 1c) complemented the cell solution. Note that strong spherical spots and weak elongated spots are simultaneously present; considering intense spots only, they can be unambiguously indexed as in-plane diffractions, taken along the [001] zone axis. The presence of forbidden spots, *h*10, is probably from the extremely small c^* value derived from the large *c* dimension and the elongation of diffraction spots along [001]* arising from the very small thickness of the sample. The presence of weak spots is a characteristic feature of superstructure, which is explained in a later part.

Crystal Structure Determination. Among the three candidate space groups, the search for a solution started from the one with the highest symmetry, *A*2/*m*. As mentioned above, each unit cell contains 4 Tb atoms and the composition is $Tb_4(OH)_8(SO_4)_2 \cdot 4H_2O$. Because the refinement of hydrogen is beyond the accuracy of powder data, we took the compound as $Tb_4O_{20}S_2$ at the starting stage. An initial model was obtained using direct

dx.doi.org/10.1021/ic200578r |*Inorg. Chem.* 2011, 50, 6667–6672

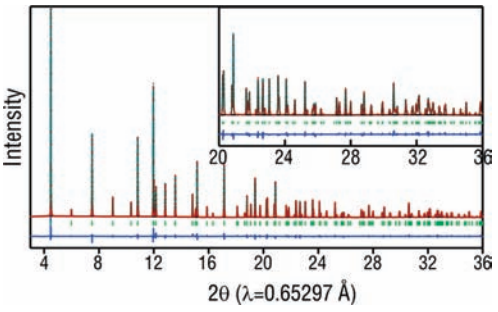

Figure 2. Rietveld plot for $Tb_2(OH)_4SO_4 \cdot 2H_2O$ in $A2/m$. The red, green, and blue lines represent the experimental, calculated, and difference profiles, respectively.

Table 1. Refined Structure Parameters for $Tb_2(OH)_4SO_4 \cdot 2H_2O$[a]

atom	site	g	x	y	z	U (Å^2)
Tb	4i	1	0.25463(9)	0.5	0.20230(2)	0.0046(1)
OH1	4i	1	0.5050(6)	0	0.1910(2)	0.009(1)
OH2	4i	1	0.8643(6)	0	0.7144(3)	0.014(1)
H_2O	4i	1	0.9003(7)	0	0.8904(3)	0.046(2)
O1	4i	1	0.4189(7)	0	0.5672(2)	0.010(1)
O2	8j	0.5	0.7317(13)	0.8278(11)	0.0413(3)	0.014(2)
S	4i	0.5	0.3950(6)	0.5	0.9812(3)	0.015(1)

[a] Space group: $A2/m$ (No. 12). Unit-cell parameters: a = 6.24528(2) Å, b = 3.71268(1) Å, c = 16.63302(6) Å, β = 90.0718(3)°. Numerals in parentheses are standard deviations.

methods embedded in EXPO2004 for heavy Tb atoms. RIETAN-2000 refinement and MEM analysis were subsequently performed for the other lighter species. Meanwhile, as the current compound shows some similarity with rare-earth hydroxide chloride of a different composition we studied before (vide ante), $Tb_2(OH)_5Cl \cdot 2H_2O$, its structure was used as a reference for the positioning of O atoms in the host layer. Since there are only 2 S atoms, the sulfur atom was initially placed on a 2-fold position. After many cycles, a good agreement between the observed and calculated X-ray powder pattern was produced. The host layer was composed of connected 9-fold polyhedra. The sulfur atom was located at a symmetry center for 2-fold rotation in the midway between the lanthanide layers. Although there were 4 O atoms around 1 sulfur atom, 2 from neighboring layers and 2 from the interlayer, they could not readily form a tetrahedral geometry of SO_4^{2-}. Furthermore, refinement of isotropic temperature factors (B) revealed unreasonably large values, 18.92 Å^2 for S and 14.21 Å^2 for the interlayer oxygens. The facts suggest possible disorder of interlayer sulfate ions. It was found that the structure model with the sulfur atom and the interlayer oxygens being displaced to a 4-fold and 8-fold position, respectively, with an occupation of 50% yielded appropriate values of thermal parameters and S−O distances. Oxygen atoms within 1.5 Å to the sulfur atom were ascribed to oxygen of SO_4^{2-}; two oxygen sites were within bond reach with 3 Tb centers, which is a common feature for hydroxyls in hydroxides; the other one close to the gallery was labeled as H_2O. The above site assignment is perfectly consistent with the nominal composition, $Tb_4(OH)_8(SO_4)_2 \cdot 4H_2O$. Further structure refinement gave satisfactory low convergence reliability indices: R_{wp} = 5.92% (S = 0.5072),

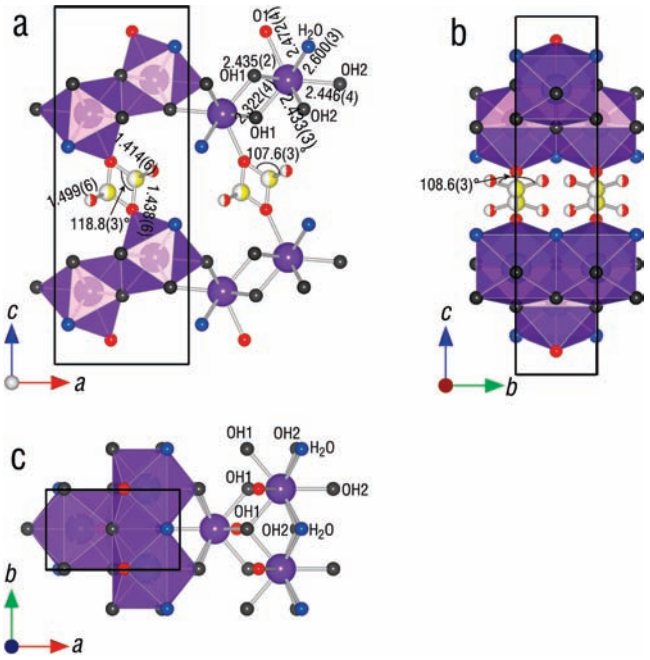

Figure 3. $Tb_2(OH)_4SO_4 \cdot 2H_2O$ cell viewed down the (a) b axis with important bonds and angles (b) a axis showing the relative shift of adjacent layers along the b axis reflecting the A-centered symmetry, and (c) c axis showing the quasi-hexagonal arrangement of Tb atoms. Color code: Tb, purple; OH, gray; H_2O, blue; O, red; S, yellow. The black lines represent the unit cell.

R_p = 4.42%, R_I = 2.01%, R_F = 1.23%, which provides strong evidence for the appropriateness of the structure model. The final full-profile Rietveld fitting of the experimental, calculated, and difference patterns is given in Figure 2.

Description of the Structure. Refined atomic positional and thermal parameters are listed in Table 1. The crystal structure determined with important bond distances and angles is shown in Figure 3. The three-dimensional electron-density distribution is visualized in the Supporting Information, which corresponds well to the atomic structure model. The key feature of the crystal structure for $Tb_2(OH)_4SO_4 \cdot 2H_2O$ is stacking of layers parallel to the (001) plane, which are rigidly bridged by bidentate sulfate groups. There is one crystallographically distinct site for Tb in the unit cell, two distinct sites for OH^-, two for O of SO_4^{2-}, and one unique site for S and H_2O. Viewing from the c axis, Tb atoms form a quasi-hexagonal network and the deviations from ideal hexagonal arrangement, especially in the c direction, gives the larger low-symmetry cell. Each Tb center is surrounded by 9 O atoms, 6 stemming from hydroxyls, 2 from H_2O molecules, and 1 from the sulfate tetrahedron. Each TbO_9 polyhedra is linked to the surrounding six TbO_9 polehedra by μ_3-OH groups and μ_2-H_2O molecules, forming an infinite two-dimensional corrugated sheet parallel to the ab plane. The TbO_9 polyhedra can be described as a distorted monocapped square antiprism with the sulfate oxygen as the cap being located on the outer edges of the corrugated sheets. The oxygen caps of two TbO_9 polyhedra from neighboring layers that point to each other form a tetrahedron for a sulfate along with two other terminal oxygen atoms in the gallery. The Tb−O (OH^-) distances range from 2.322(4) to 2.446(4) Å, a Tb−O(SO_4^{2-}) bond length of 2.472(4) Å, and a Tb−O(H_2O) distance of 2.600(3) Å. The average is 2.46 Å, which is comparable to the sum of radii given by Shannon's table,

dx.doi.org/10.1021/ic200578r |Inorg. Chem. 2011, 50, 6667–6672

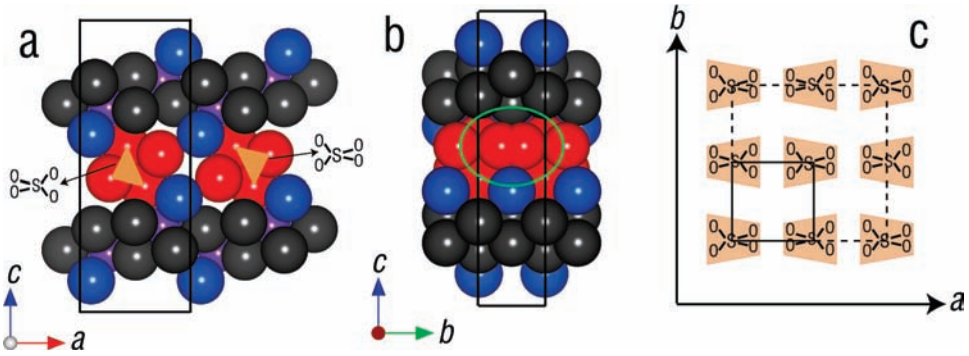

Figure 4. Space-filling views of the structure model for $Tb_2(OH)_4SO_4 \cdot 2H_2O$ with both configuration possibilities of SO_4^{2-} included. The gray, blue, and red balls represent OH, H_2O, and sulfate O, respectively. (a) To differentiate the two configurations at the half-occupancy site, the four oxygen atoms composing one sulfate unit are marked with orange triangles and the corresponding frame sketches are drawn. Obviously there is enough space for SO_4^{2-} to be in opposite orientation along [100]. (b) The green circle marks the collision of oxygen atoms if both neighboring SO_4^{2-} units along [010] point to the same direction. (c) Sulfate configurations in the *ab* plane showing a face-centered feature. The solid and broken lines mark unit cell and super cell, respectively.

2.445 Å.[30] As the range of hydrogen-bond distances for O···O in inorganic salts was given to be 2.49(6)−3.15(6) Å,[31] hydrogen bonding is involved between coordinated oxygen atoms of the main layer and the sulfate group as confirmed by O···O distances of 2.797(7)−2.936(7) Å. There is also a suggestion of a free or weak hydrogen bond for OH2, whose distance with the oxygen atoms in the gallery is beyond 3.2 Å. This may explain the observation of two sharp characteristic peaks at 3613 and 3477 cm^{-1} in the infrared spectra ascribed to OH stretching modes free from hydrogen bonding.[22]

The coordinated water molecules always play an important role in stabilizing the structure of rare-earth compounds, especially in layered materials. In $Ln_2(OH)_5X \cdot mH_2O$, water molecules point toward the gallery and water loss generally results in contraction or complete collapse of the layered structure.[6] Both $Ln(OH)_2NO_3 \cdot H_2O$ and $Ln(OH)_2NO_3$ are crystalline, and the oxygen of nitrate fills the active empty site left by water removal, which makes nitrate act as a monodentate ligand in $Ln(OH)_2NO_3 \cdot H_2O$ and bidentate ligand in $Ln(OH)_2NO_3$.[1] For the title compound, $Tb_2(OH)_4SO_4 \cdot 2H_2O$, the water molecules are not evaporated unless being heated to 200−300 °C.[22] The obtained anhydrous phase, $Tb_2(OH)_4SO_4$, was insufficiently crystalline for structural studies. However, one can note that the basal spacing is shifted from 8.8 to 6.8 Å. Possibly as happens in $Ln(OH)_2NO_3$, in which a terminal oxygen of NO_3^- fills the site left by water removal, the free O of the SO_4 group binds to the lanthanide center in the host layer, yielding a more compact structure.

Every second layer is shifted by 1/2 the length of the *b* axis, which reflects the *A*-centered symmetry. The sulfate groups in the gallery act as bidentate bridges to connect the neighboring layers. Notably, the shape of the sulfate units is distorted from a regular tetrahedron. As might be expected, the distance of S to the sulfate coordinated oxygen ($S-O1_{coor}$ = (1.414(6)/1.438(6) Å) is shorter than that to the terminal oxygen ($S-O2_{term}$ = 1.499(6) Å). The angles O1−S−O1, O2−S−O2, and O1−S−O2 are 118.8(3)°, 108.6(3)°, 107.0(3)°/107.6(3)° with an average of 109.4°, which suggests the sulfate ion is distorted into a quasi-C_{2v} symmetry.

Ordering of Sulfate Orientation. Since sulfate S and the remaining two oxygen atoms in the gallery are displaced to two split positions with an occupancy probability of 1/2 for each, there are two possible configurations for each sulfate unit. The available space in the gallery should strongly influence the instantaneous positions of SO_4^{2-}. In this sense, it is worth checking the possible positioning of sulfate ions based on steric considerations. Figure 4a and 4b present the models in space-filling mode containing sulfate tetrahedra of both possible configurations in the [100] and [010] directions, respectively. Apparently the space is enough for sulfate ions to be either in the same or in opposite directions along [100], whereas SO_4^{2-} would collide if being located in the same direction along [010] as marked by the green circle in Figure 4b. Therefore, the configuration of SO_4^{2-} has to be alternated in the *b* direction, whereas both identical and alternate configurations are geometrically allowed in the *a* direction. The observation of superstructure reflections in the SAED pattern (vide ante) corroborated the sulfate orientation ordering, being alternated along both [100] and [010] directions. The ordering gives a supercell with the doubled cell parameters 2*a* and 2*b*. Only *h*/2 *k*/2 0 ($h + k = 2n$) superstructure reflections were found because the ordered sulfate ions exhibit a face-centered feature (Figure 4c). Note that the superspots show extended diffuse streaking along *a**, indicative of short ordering length along [100]. This is in good accordance with the fact that the SO_4^{2-} in both orientations are geometrically allowed, and consequently, the neighboring SO_4^{2-} might occasionally be orientated in the same direction. Since only one-half of the oxygen positions are occupied, the compound can be considered as a micro- or mesoporous material and be used as capture and storage media. However, the pore is not accessible because of the alternating configuration of sulfate ions along the *b* direction, and as a consequence, adsorption of even small molecules such as H_2O becomes sterically hindered (Supporting Information).

The staggered layer composed of distorted 9-fold Tb monocapped square antiprism and superstructure from sulfate ordering are certainly not unique to this structure, but the bridge of adjacent layers through bidentate SO_4^{2-} is unprecedented. Similar stacks of a $Ln_2O_2^{2+}$ layer and a sulfate (SO_4^{2-}) layer were found in $Ln_2O_2SO_4$, but each sulfate oxygen is coordinated with two lanthanide atoms, and therefore, more condensed layers are formed. The structure feature gives hints for structure engineering, for example, inorganic−organic hybrid compounds in which inorganic layers are connected by organic chains with

dx.doi.org/10.1021/ic200578r |*Inorg. Chem.* 2011, 50, 6667–6672

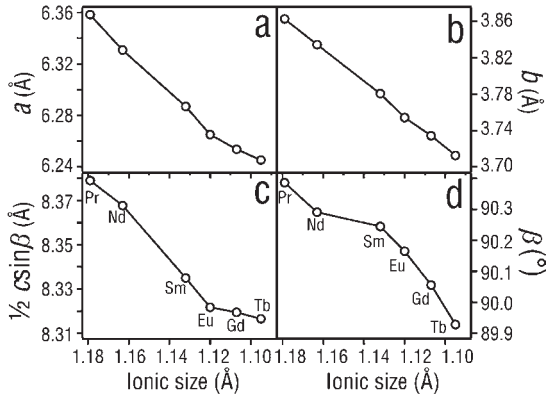

Figure 5. Correlation of the lattice parameters (a) a, (b) b, (c) gallery height ($1/2c\sin\beta$), and (d) β with cationic sizes. Supplementary angle 89.9282° is used for Tb sample to illustrate the decreasing trend of the β parameter. The standard deviations are on the 5th and 3rd decimal place for axes dimensions (a, b, and c) and β, respectively, and are thus invisible.

Table 2. S−O Bond Distances in SO_4^{2-} Tetrahedra along the Lanthanide Series

S−O bond distance (Å)	S−O1	S−O2	difference between two S−O1 distances [Δ(dis)]
Pr	1.375(8)/1.467(9)	1.477(7)	0.092
Nd	1.387(9)/1.473(9)	1.481(8)	0.086
Sm	1.402(8)/1.451(9)	1.484(8)	0.049
Eu	1.431(8)/1.408(9)	1.476(8)	0.023
Gd	1.415(9)/1.397(11)	1.468(9)	0.018
Tb	1.414(6)/1.438(6)	1.499(6)	0.024

sulfate heads, being similar to zirconium phosphonates.[32] Furthermore, the compounds having long-chain supported gallery are expected to possess more porosity for storage or work as channel.

Structural Evolution. Study of lanthanide compounds across the series is useful for examining the effect of the reducing metal ionic radii on the crystal structure. Analysis of the X-ray powder patterns of other members indicated that they can be indexed on similar monoclinic unit cells. The cell parameters were first refined with APPLEMAN. Rietveld refinements of these materials were carried out starting from the solution found for the Tb sample. Final convergence was achieved for all samples. Crystallographic details and the final Rietveld fits of the powder X-ray data along with the table of lattice parameters and unit-cell volume for all samples are gathered in the Supporting Information. The evolution of the deduced lattice parameters across the series is illustrated in Figure 5. The in-plane parameters, a and b, decrease nearly monotonically with the decreasing cation size/increasing atomic number, which reflects the lanthanide contraction. For gallery height, $1/2c\sin\beta$, it also shrinks with an increase in atomic number, with the slope becoming gradual after Eu. It is interesting to note that compared to the contraction in a and b axes showing an slope of 1.344 and 1.787, respectively, the c axis declines to a lesser extent, only at 0.971 from Pr to Eu and 0.208 from Eu to Tb, which is because the shrinkage of c dimensions is largely constrained by the rigid pillaring of SO_4^{2-}. The β parameter, which characterizes

Table 3. O−S−O Angles along the Lanthanide Series

O−S−O angle (deg)	O1−S−O1	O1−S−O2	O2−S−O2
Pr	120.4(4)	107.2(4)/105.8(4)	110.3(4)
Nd	122.3(4)	106.4(4)/106.4(4)	108.3(4)
Sm	122.5(3)	107.8(4)/106.1(4)	105.4(4)
Eu	121.5(3)	106.7(4)/107.1(4)	106.9(4)
Gd	121.0(4)	106.6(4)/106.8(4)	108.6(4)
Tb	118.8(3)	107.0(3)/107.6(3)	108.6(3)

the degree of distortion from orthorhombic symmetry, also decreases with diminishing sizes of the lanthanide cations, though in very small steps, from 90.387(1)° for Pr, 90.291(1)° for Nd, 90.245(1)° for Sm, 90.165(1)° for Eu, 90.055(2)° for Gd, and to 90.0718(3)° or its supplementary angle of 89.9282(3)° for Tb. In accordance with the contraction of unit cells, the average Ln−O distances in a polyhedron show a similar decreasing trend (Supporting Information).

The changes of S−O distances and O−S−O angles along the series are tabulated in Tables 2 and 3. The minimum S−O bond length, 1.375(8) Å, is shorter than the normal S−O distance but still well within 3σ of the range of 1.44(4)−1.53(4) Å given in the "International Tables of Crystallography" for the SO_4^{2-}.[31] While the S−$O2_{term}$ distances are little affected by the changing size of Ln^{3+} cations showing consistent values around the average (1.49 Å) throughout the six compounds, S−$O1_{coor}$ lengths are shortened and fluctuate across the series. It is noteworthy that the distances of S to $O1_{coor}$ atoms of the neighboring layers are different, generating a more distorted SO_4^{2-} tetrahedron. We determine the degree of distortion, Δ(dis), with the difference value, which is included in Table 2. Interestingly, the degree of distortion Δ(dis) becomes progressively less marked from Pr to Gd and exhibits an increase again for Tb. The SO_4^{2-} tetrahedra in Gd sample deviate the least, and those in Pr sample are the most distorted, in good accordance with infrared observations that the ν_3 mode of SO_4^{2-} was the most asymmetric.[22] SO_4^{2-} groups rarely show distortions from regular tetrahedra in most crystal structures because of the strong S−O bond strength.[33] The distortion observed in the currently studied structures probably arises from the fact that Ln^{3+} form stronger bonds with sulfate oxygen because they are rather hard acceptors.[34] Across the series, Gd^{3+} is the most stable with a half-filled 4f electron shell, showing the lowest tendency to accept ions, and therefore its bond strength is expected to be weak with the least influence on the geometry of sulfate ions. The O−S−O angles in a regular tetrahedron are expected to be 109.47°. O1−S−O2 and O2−S−O2 angles are close to the ideal value, ranging from 106.1(4)° to 110.3(4), whereas O1−S−O1 angles deviate significantly from the ideal tetrahedral angle and are widened to 118.8(3)−122.5(3)°, which is consistent with the previous report that shortening in a S−O bond leads to an increase in the angles.[33]

CONCLUSIONS

The present study deals with structural determination of a new family of rare-earth hydroxides $Ln_2(OH)_4SO_4\cdot 2H_2O$ (Ln = Pr, Nd, Sm, Eu, Gd, Tb) from powder diffraction. The isostructural compounds are crystallized in a monoclinic symmetry ($A2/m$) and composed of lanthanide hydroxide layers pillared by bidentated sulfate ions. Generally, SO_4^{2-} is distorted with shortened distances of S to the sulfate oxygen coordinated with the host

dx.doi.org/10.1021/ic200578r |Inorg. Chem. 2011, 50, 6667–6672

layers. Furthermore, the structure shows a supercell $a' = 2a$, $b' = 2b$ originating from the orientation ordering of sulfate ions, which was corroborated by SAED observations. Examinations of structural trends as a function of the progressive reduction in the sizes of Ln cations revealed that, following the well-known lanthanide contraction, not only in-plane dimensions, a and b, but also gallery height ($1/2\ c\sin\beta$) and monoclinic angle (β) decrease as the size of Ln centers decreases across the series. This structural study is essential, and it provides hints for possible structure engineering of an organic−inorganic framework in which the inorganic layers are pillared by organic ions with similar sulfate heads.

■ ASSOCIATED CONTENT

Supporting Information. Electron-density distribution map of the Tb sample, pore geometry and change of sample weight as a function of relative humidity, crystallographic details and final Rietveld plots of all members, table of lattice parameters and cell volumes of all members, and the change of Ln−O distances along the lanthanide series. This material is available free of charge via the Internet at http://pubs.acs.org.

■ AUTHOR INFORMATION

Corresponding Author
*Fax: (+81) 29-854-9061. E-mail: SASAKI.Takayoshi@nims.go.jp.

■ ACKNOWLEDGMENT

This work was supported by the World Premier International Center Initiative (WPI Initiative) on Materials Nanoarchitectonics, MEXT, Japan and CREST of the Japan Science and Technology Agency (JST).

■ REFERENCES

(1) Newman, S. P.; Jones, W. *J. Solid State Chem.* **1999**, *148*, 26–40.
(2) Geng, F.; Ma, R.; Sasaki, T. *Acc. Chem. Res.* **2010**, *43*, 1177–1185.
(3) Gándara, F.; Perles, J.; Snejko, N.; Iglesias, M.; Gómez-Lor, B.; Gutiérrez-Puebla, E.; Monge, M. Á. *Angew. Chem., Int. Ed.* **2006**, *45*, 7998–8001.
(4) McIntyre, L. J.; Jackson, L. K.; Fogg, A. M. *Chem. Mater.* **2008**, *20*, 335–340.
(5) Geng, F.; Xin, H.; Matsushita, Y.; Ma, R.; Tanaka, M.; Izumi, F.; Iyi, N.; Sasaki, T. *Chem.—Eur. J.* **2008**, *14*, 9255–9260.
(6) Geng, F.; Matsushita, Y.; Ma, R.; Xin, H.; Tanaka, M.; Izumi, F.; Iyi, N.; Sasaki, T. *J. Am. Chem. Soc.* **2008**, *130*, 16344–16350.
(7) Poudret, L.; Prior, T. J.; McIntyre, L. J.; Fogg, A. M. *Chem. Mater.* **2008**, *20*, 7447–7453.
(8) Geng, F.; Matsushita, Y.; Ma, R.; Xin, H.; Tanaka, M.; Iyi, N.; Sasaki, T. *Inorg. Chem.* **2009**, *48*, 6724–6730.
(9) Lee, K.-H.; Byeon, S.-H. *Eur. J. Inorg. Chem.* **2009**, 929–936.
(10) Lee, K.-H.; Byeon, S.-H. *Eur. J. Inorg. Chem.* **2009**, 4727–4732.
(11) Hu, L.; Ma, R.; Ozawa, T. C.; Sasaki, T. *Angew. Chem., Int. Ed.* **2009**, *48*, 3846–3849.
(12) Hu, L.; Ma, R.; Ozawa, T. C.; Geng, F.; Iyi, N.; Sasaki, T. *Chem. Commun.* **2008**, 4897–4899.
(13) Gándara, F.; Puebla, E. G.; Iglesias, M.; Proserpio, D. M.; Snejko, N.; Monge, M. Á. *Chem. Mater.* **2009**, *21*, 655–661.
(14) Yoon, Y.-S.; Lee, B.-I.; Lee, K. S.; Im, G. H.; Byeon, S.-H.; Lee, J. H.; Lee, I. S. *Adv. Funct. Mater.* **2009**, *19*, 3375–3380.
(15) Lee, B.-I.; Lee, K. S.; Lee, J. H.; Lee, I. S.; Byeon, S.-H. *Dalton Trans.* **2009**, 2490–2495.
(16) Klevtsova, R. F.; Klevtsov, P. V. *J. Struct. Chem.* **1967**, *7*, 524–527.
(17) Klevtsova, R. F.; Glinskaya, L. A. *J. Struct. Chem.* **1969**, *10*, 408–410.
(18) Mullica, D. F.; Sappenfield, E. L.; Grossie, D. A. *J. Solid State Chem.* **1986**, *63*, 231–236.
(19) Louër, M.; Louër, D.; Delgado, A. L.; Martinez, O. G. *Eur. J. Solid State Inorg. Chem.* **1989**, *26*, 241–253.
(20) Zehnder, R. A.; Clark, D. L.; Scott, B. L.; Donohoe, R. J.; Palmer, P. D.; Runde, W. H.; Hobart, D. E. *Inorg. Chem.* **2010**, *49*, 4781–4790.
(21) Haschke, J. M. *J. Solid State Chem.* **1988**, *73*, 71–79.
(22) Liang, J.; Ma, R.; Geng, F.; Ebina, Y.; Sasaki, T. *Chem. Mater.* **2010**, *22*, 6001–6007.
(23) Visser, J. W. *J. Appl. Crystallogr.* **1969**, *2*, 89–95.
(24) Boultif, A.; Louër, D. *J. Appl. Crystallogr.* **1991**, *24*, 987–993.
(25) Werner, P.-E.; Eriksson, L.; Westdahl, M. *J. Appl. Crystallogr.* **1985**, *18*, 367–370.
(26) Appleman, D. E.; Evans, H. T.; Handwerker, D. S. *Program X-ray*; Geological Survey, U.S. Department of the Interior: Washington, DC, 1966.
(27) Altomare, A.; Caliandro, R.; Camalli, M.; Cuocci, C.; Giacovazzo, C.; Moliterni, A. G. G.; Rizzi, R. *J. Appl. Crystallogr.* **2004**, *37*, 1025–1028.
(28) Izumi, F.; Ikeda, T. *Mater. Sci. Forum* **2000**, *321−324*, 198–203.
(29) Izumi, F. *J. Ceram. Soc. Jpn.* **2003**, *111*, 617–623.
(30) Shannon, R. D. *Acta Crystallogr.* **1976**, *A32*, 751–767.
(31) *International Tables for X-Ray Crystallography*; The Kynoch Press: Birmingham, England, 1968; Vol. III.
(32) Gao, G.; Hong, H.-G.; Mallouk, T. E. *Acc. Chem. Res.* **1992**, *25*, 420–427.
(33) Brown, I. D. *Acta Crystallogr.* **1973**, *B29*, 1979–1983.
(34) Bünzli, J.-C. G. *Acc. Chem. Res.* **2006**, *39*, 53–61.